# Optical PAyload for Lasercomm Science (OPALS) Link Validation

Abhijit Biswas[1], Bogdan V. Oaida, Kenneth S. Andrews, Joseph M. Kovalik, Matthew J. Abrahamson, and Malcolm W. Wright
Jet Propulsion Laboratory, California Institute of Technology, 4800 Oak Grove Dive, Pasadena, CA 91109.

## ABSTRACT

Recently several day and nighttime links under diverse atmospheric conditions were completed using the Optical Payload for Lasercomm Science (OPALS) flight system on-board the International Space Station (ISS). In this paper we compare measured optical power and its variance at either end of the link with predictions that include atmospheric propagation models. For the 976 nm laser beacon mean power transmitted from the ground to the ISS the predicted mean irradiance of 10's of microwatts per square meter close to zenith and its decrease with range and increased air mass shows good agreement with predictions. The irradiance fluctuations sampled at 100 Hz also follow the expected increase in scintillation with air mass representative of atmospheric coherence lengths at zenith at 500 nm in the 3-8 cm range. The downlink predicted power of 100's of nanowatts was also reconciled within the uncertainty of the atmospheric losses. Expected link performance with uncoded bit-error rates less than 1E-4 required for the Reed-Solomon code to correct errors for video, text and file transmission was verified. The results of predicted and measured powers and fluctuations suggest the need for further study and refinement.

**Keywords:** ISS, lasercomm, downlink, bit-error-rate, beacon, 1550 nm, atmospheric scintillation

## 1. INTRODUCTION

The Optical Payload for Lasercomm Science (OPALS)[1-4] technology demonstration of optical communication from the ISS was completed between June and October of 2014. During this time 18 successful links were demonstrated downlinking data at 33 - 50 Mb/s. Half of these passes were daytime passes. The key elements of the OPALS demonstration were the Flight System (FS) deployed on an external nadir pointing location of the ISS; the Ground System (GS) located at NASA's Optical Communication Telescope Laboratory near Wrightwood, CA; and the Mission Operations System (MOS) located on the Jet Propulsion Laboratory campus in Pasadena, CA. Operations were coordinated through the Huntsville Operations Support Center (HOSC) at the NASA Marshall Space Flight Center (MSFC). Video, text and telemetry files stored in the OPALS FS avionics memory on the ISS were successfully downlinked during the demonstration.

In this paper we will present power and bit-error rate measurements and discuss the extent of agreement with analytical predictions. The details of link acquisition are presented elsewhere[5] in this volume. Each successful link involved the transmission of a 976 nm laser beacon transmitted from the GS toward the ISS using a blind pointing table generated approximately an hour prior to contact and using ISS position data telemetered to the ground. At the start of a scheduled pass the FS would also blind-point to the ground using its two-axis gimbal driven with on-board predicts. Blind pointing resulted in the ground laser being acquired on the FS charge coupled device (CCD) camera. The FS then transitioned into a closed-loop track by controlling the gimbal to maintain the laser spot centered in the camera field-of-view (FOV). Closed loop FS tracking resulted in the 1550 nm downlink laser beam emitted from a collimator co-bore-sighted to the camera to point back at the GS. The GS telescope control transitioned from blind-pointing to closed loop tracking with the acquired downlink signal and centered the downlink beam on a communication detector.

In principle low-Earth orbiting spacecraft can be tracked almost from horizon-to-horizon from the ground with the OCTL telescope. OPALS demonstrated reliable tracking from approximately 6-10-deg elevation when tracking the sun-illuminated ISS, without any atmospheric refractive correction, both during night and day. However, ISS safety

[1] Abhijit.Biswas@jl.nasa.gov; phone (818)-354-2415; fax (818)-393-6142;

restrictions prevent illumination of ISS structure, panels or docked assets, at any time. The field-of-regard of the two-axis gimbal on the ISS was restricted to comply with this requirement. As a result the OPALS gimbal could slew +75° to -35° around the axis aligned to the ram direction of the ISS and +40° to -1° in the direction normal to the ram direction. The OPALS demonstration was carried out within these constraints and the contact times though short, typically 150 sec, allowed measurements through varying air-mass and under a diverse set of conditions. Nominal passes allowed link acquisition as the spacecraft was rising over an elevation range of 15-25° above the GS, through the peak elevation and down to an elevation angle of approximately 40°. In off-nominal configurations encountered periodically as a part of docking operations the ISS is flipped around the yaw axis and this allows links to be acquired near the peak elevation angle and tracked down to elevation angles as low as 12°.

The mean 976 nm laser beacon power and its fluctuations were sensed by the CCD camera operating at a frame rate of 100 Hz. As we will show, CCD camera measurements allowed an evaluation of the mean power and its fluctuations over a range of air-mass even though the dynamic range and temporal sampling rates were somewhat limited. Additionally, 1Hz image frames were also stored and have been analyzed elsewhere[6] in this volume to evaluate upwelling radiance under different daytime conditions. Mean detected 1550 nm downlink power on the ground with bit-error rates were also measured and are reported.

The remainder of this paper is organized as follows. In Section 2 the beacon power received by the OPALS FS camera and its fluctuations are presented and compared to analytical predictions. Section 3 will present the downlink power and bit-error rate measurements. Section 4 will conclude the paper.

## 2. OPALS BEACON RESULTS

### 2.1 OPALS CCD Camera Measurements of Beacon Flux

The OPALS FS camera operates at a frame rate of 100 Hz. Based on characterization of day and nighttime background measurements made during commissioning the integration times were set to 0.5 milliseconds (ms) for nighttime passes and 0.2 ms for daytime passes. Setting the integration time higher for daytime passes resulted in vulnerability to noise[5] contributed by upwelling radiance. The threshold for detecting the beacon was typically set to digital number (DN) of 100 for daytime passes.

Figure 1 shows the raw camera recorded digital numbers for a nighttime pass on July21, 2014.

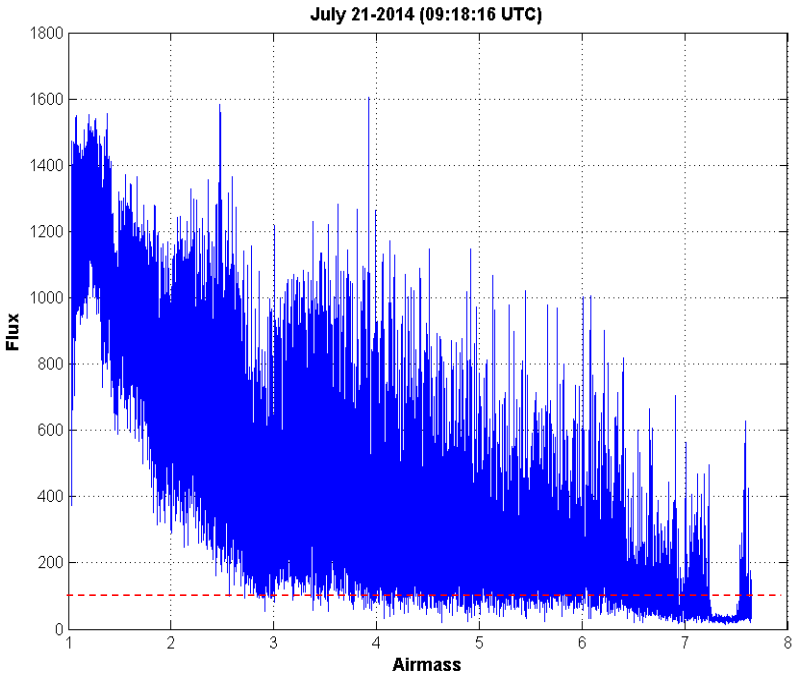


Figure 1. The 100 Hz digital number (DN) recorded by the OPALS FS camera on July 21, 2014.

The quantity plotted is the background subtracted digital sum of pixels in an 8 × 8 sub-window. The background is estimated as an average of the perimeter pixels. The beacon is identified by setting a threshold of 100 DN shown by the dashed horizontal line. As reported elsewhere[5] there were occasions when this threshold could be exceeded by glint caused by near specular reflection on a few instances.

The Kasten and Young model[7] was used to calculate the air-mass plotted along the abscissa of Figure 1. The dependence of air-mass on the zenith angle (ZA) is shown in Equation 1.

$$\text{Air} - \text{Mass} = \frac{1}{\cos(\text{ZA}) + 0.50572(6.07995^{\circ} + 90 - \text{ZA})^{-1.6364}} \quad (1)$$

Dips in beacon flux at an air-mass of 3 and 1.5 are shown in Figure 1. These are an artifact of the four beamlets[5] rotating relative to the primary mirror and getting partially blocked by the struts that hold the secondary mirror on the telescope. Generally the beacon dips did not interrupt the link or cause degradation in link performance.

The mean flux sensed by the camera was compared to link predictions. Mean measurements from a few day and night passes were used for this evaluation.

### 2.2 Comparison of Mean Beacon Flux to Link Predictions

Table 1 shows a tabulation of link parameters that contribute to irradiance at the OCTL zenith

**TABLE 1** Link parameters for zenith irradiance for two different beam divergences used for OPALS

| | Low Divergnce | | | | High Divergence | | | |
|---|---|---|---|---|---|---|---|---|
| **LASER TRANSMITTER** | | | | | | | | |
| Uplink Wavelength | | | 976 | nm | | | 976 | nm |
| Uplink Laser Linewidth | | | 0.4 | nm | | | 0.4 | nm |
| Average Transmitted Power | 9.7 | dBW | 9.25 | W | 9.7 | dBW | 9.25 | W |
| **FREE-SPACE GAIN/LOSS** | | | | | | | | |
| Transmitter Gain | 74.2 | dB | | | 71.5 | dB | | |
| Beam Divergence | | | 1100 | mrad | | | 1500 | mrad |
| Tranmsitter Optical Loss | -4.4 | dB | | | -4.4 | dB | | |
| Zenith Angle | | | 0 | deg | | | 0 | deg |
| Air Mass | | | 1.00 | | | | 1.00 | |
| Atmospheric Loss/Transmittance | 0 | dB | 1 | | 0 | dB | 1 | |
| Atmospheric Strehl_Loss | -0.01 | | 3 | cm | -0.006 | | | |
| Range Loss/Range | -254.61 | dB | 430 | km | -254.61 | dB | 430 | km |
| Mean Irradiance at Aperture | | | 4.0E-05 | $W/m^2$ | | | 2.2E-05 | $W/m^2$ |

The mean beacon divergences used during the OPALS demonstration were 1.1 mrad and 1.5 mrad. Table 1 displays the zenith irradiance of 22-40 $\mu W/m^2$ would result assuming no atmospheric transmission losses. The beacon transmitted from the OPALS GS consisted of 4-beamlets and perfect overlap and alignment would result in the irradiance shown if there were no atmospheric transmission losses. The gains and losses resulting in the zenith irradiance shown in Table1 are fixed over the duration of the pass. During a pass the range to the ISS and the atmospheric transmission are changing continuously and would have to be accounted for in order to derive the dependence of irradiance on instantaneous range and zenith angle.

The drop in irradiance predicted due to increase in ISS range is shown in Figure 2a. For determining the dependence atmospheric attenuation, both as a function of zenith angle and atmospheric conditions, a number of models were investigated using MODTRAN[8]. These were rural visibility with 23 km and 5 km visibility. Aerosol models with no clouds or rain (NCNR) and 1 km thick sub-visual cirrus (SVC) 10 km altitude. Additionally, the Desert Extinction model with an average wind-speed of 2m/s was used. Figure 2b shows the predicted variation in the atmospheric

attenuation in decibels (dB). The atmospheric spectral transmission was integrated over the bandwidth of narrow band-pass filter used in front of the camera. This integrated spectral transmission is shown plotted as a function of air-mass in Figure 2b.

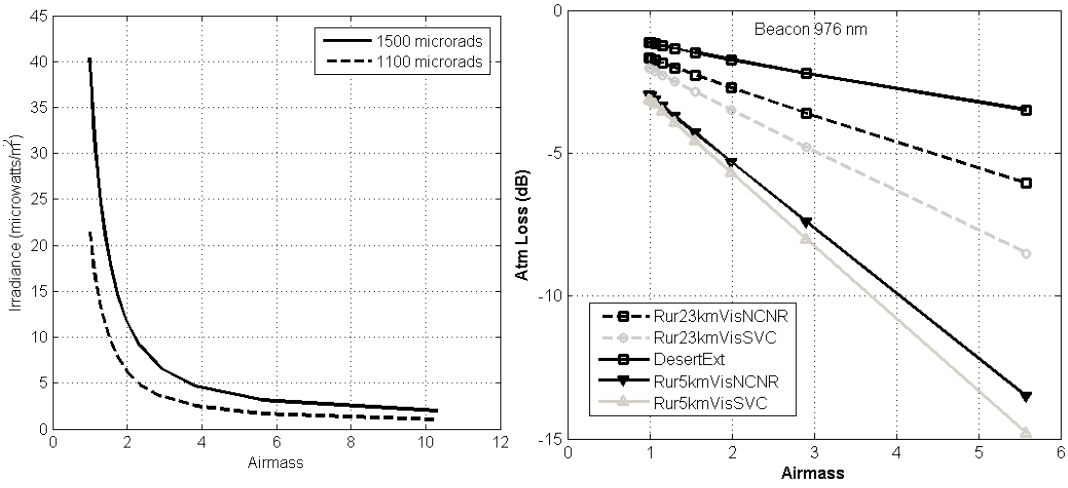


(a) (b)

Figure 2. (a) Decrease in irradiance incident on ISS due to increase in range; (b) Variation of atmospheric loss in dB predicted by different atmospheric transmission models – rural visibility of 23 and 5 km with (i) no clouds or rain (Rur23kmVisNCNR) and (ii) sub-visual cirrus (SVC) and Desert Extinction.

### 2.3 Comparison of Predictions and Measurements

Two typical night passes were used for comparison of measurements and predictions. The combination of longer integration time and absence of additive noise from upwelling radiance contributes to higher beacon fluxes and allows longer contacts that cover higher air-mass. Figure 3 shows the mean beacon flux for the July 21, 2014 and June 11, 2014 nighttime passes. Of these the July 21 pass was acquired at a high elevation angle and tracked as a function of increasing air-mass. The mean flux shown corresponds to data shown in Figure 1. The June 11, 2014 pass was initiated at lower elevation (approximately 5-10°) and tracked as the air-mass decreased.

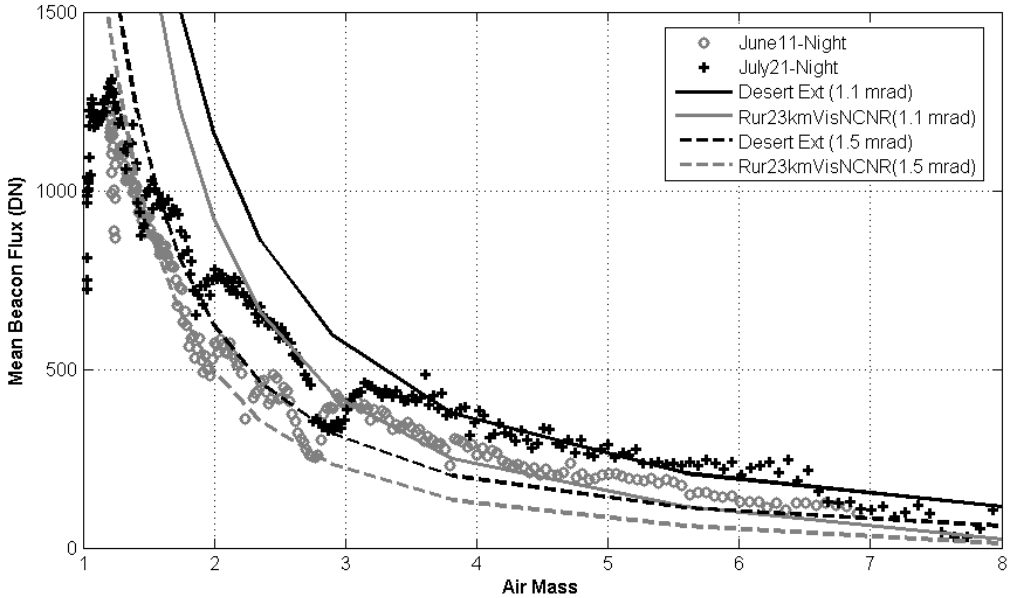


Figure 3. Comparison of typical night passes compared to the predicted DN flux on the camera.

For both the passes the beacon flux on either side of the minimum air-mass (peak elevation) displayed asymmetry in measured flux. This is not shown and the exact reason for the asymmetry is under study.

The mean beacon fluxes in Figure 3 are compared to the predicted DN flux using solid lines. The solid lines were computed by using the product of the irradiance and atmospheric transmission as a function of range (or air-mass) i.e. the product of the functions shown in Figure 2a and Figure 2b using the Desert extinction and the rural 23 km visibility with no clouds or rain. The resulting irradiance was converted to DN using a calibration curve that was measured on the ground during the integration and test of the OPALS FS. This number was further scaled by the integration time of 0.5 milliseconds and the camera gain used relative to the conditions under which ground tests were performed.

The desert extinction and rural 23 km visibility models serve as reasonable bounds. The solid lines represent the narrow 1.1 mrad beacon while the dashed lines represent the 1.5 mrad beam. Note that the June 11 pass used the wider beacon while the July 21 pass used the narrower beacon. Within the uncertainty of misalignment and perfect overlap between the 4-beacon beamlets and the atmospheric conditions on the days chosen the agreement is good. The deviation of the measurements from the model at lower air-masses is noteworthy suggestive of camera pixel saturating and limiting the dynamic range of the measurement, however, a compelling argument for this is lacking at this time. An alternate and perhaps controversial interpretation of Figure 3 is better agreement to Desert extinction at higher air-mass and to the 23 km visibility at lower air-mass, in other words suggesting that single atmospheric model does not hold over the range of air-masses sampled.

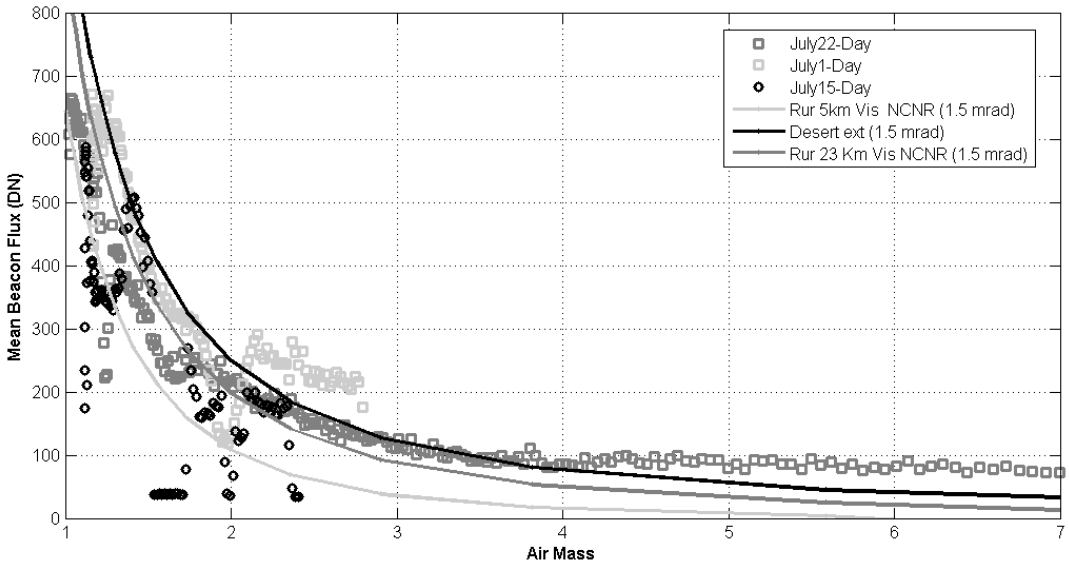


Figure 4. Day beacon measurements compared to link model.

Figure 4 shows daytime measurements made on July 1, July 15 and July 22. Of the three measurements shown only July 22 used a 1.1 mrad beam divergence. Note that the reduced integration time of 0.2 milliseconds is factored resulting in the overall mean fluxes being lower compared to nighttime measurements. Furthermore, typical daytime passes maintained contact over a lower range of air-mass with the July 22 pass being somewhat of an exception due to the off-nominal configuration of the ISS as described above. The July 15 measurements (black circles) were made through patchy clouds contributing to significant variation in the mean flux with drop-outs around air-mass of 1.75 from which the link recovered.

The solid lines are a few atmospheric models that compared reasonably to the measurements. A noteworthy feature of the comparison in Figure 4 is that even though the July 22 measurement used a narrower beam divergence it lies between the measurements of the wider beacons contrary to expectation. The July 22 measurement could not be reconciled with stronger attenuation models while accounting for the narrower beam divergence. In general the day measurements show more significant deviations from the models at larger air-masses. We offer no explanation for this observation at this time, though the suggestion that additive noise backgrounds bias the mean beacon flux upward is made.

To summarize, then an initial assessment of the measured mean beacon flux by the OPALS FS camera to atmospheric transmission predicted by MODTRAN shows better agreement for nighttime passes than the daytime passes studied in this report. The results indicate that the generally the expected variation with range and air-mass are observed. Questions remain about the atmospheric conditions to choose and whether the conditions chosen can be applied over a large range of air-mass. The case can certainly be made however, that measurements can be bounded by the models and can be used for effective designs.

### 2.4 Observed Beacon Irradiance Fluctuations on OPALS CCD Camera

As shown in Figure 1 the beacon flux sensed by the OPALS FS camera at a sample rate of 1 Hz shows significant fluctuations. Figure 5 shows the normalized variance for some typical passes versus air mass out to an air mass of 4. For air masses exceeding 4 the mean flux is weak and the normalized variance is restricted by the dynamic range of the camera due to its noise floor.

The measured normalized variance increases with air-mass. The solid lines are models of scintillation index calculated for 4 incoherently averaged laser beams when the atmospheric coherence length r0 is 3 cm 5 cm and 8 cm. The r0 values correspond to values at zenith, at 500 nm wavelength, appropriately scaled for wavelength and air-mass. Here once again the model indicates qualitative agreement though there is significant deviation observed at lower air mass once again lending credence to the suggestion made earlier that a single atmospheric model may not be adequate over a large air-mass range.

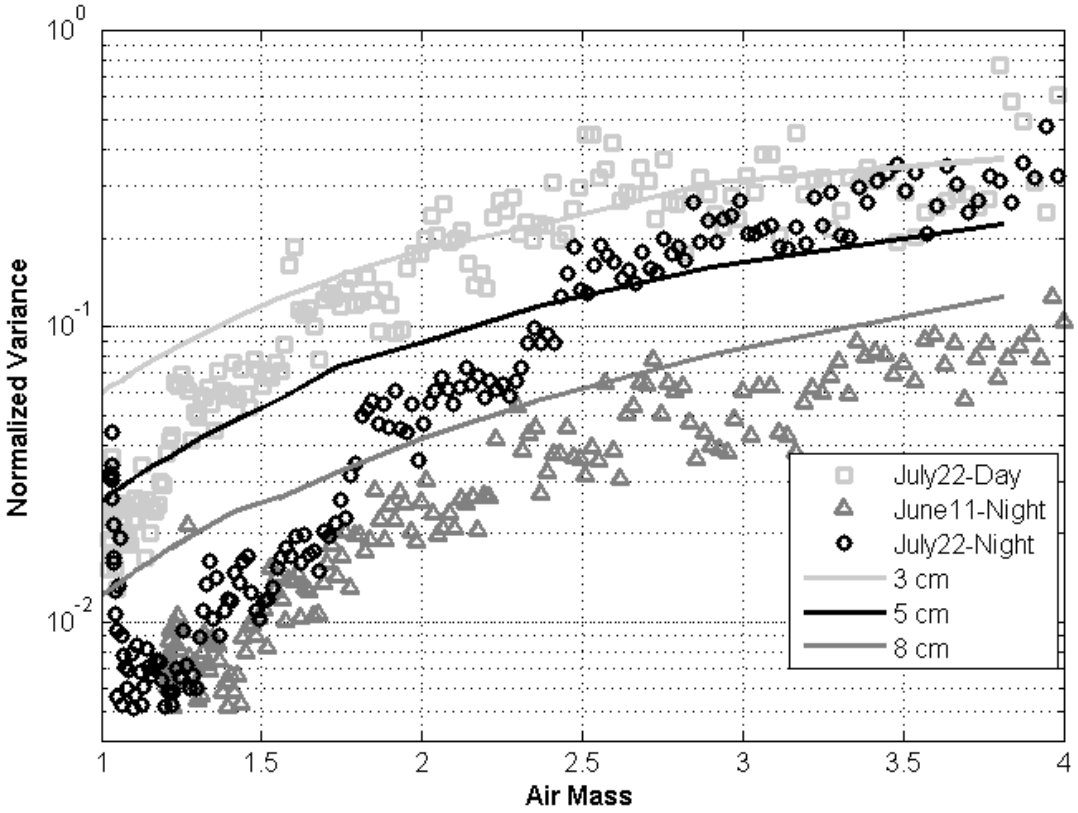


Figure 5. Normalized variance computed for the passes on July 21 (Night), July 21 (Day) and June 11 (Night).

Further refinement of the models for better agreement with measurements or understanding the reason for the deviation is needed.

Figure 6 shows a comparison of the distribution of the camera measured beacon flux for July 21 and June 11 data. The distributions were fitted to a lognormal function and consistent with the increasing normalized variance as a function of air mass the distribution also changes from a “gaussian-like” to “gamma-gamma-like” distributions as expected for weak to strong turbulence as the air-mass changes.

## 3. DOWNLINK MEASUREMENTS

Downlink power received was compared to the link budget predictions. A detailed analysis with atmospheric models as was done for the beacon is pending. Figure 7 shows a comparison of the measured power on a typical pass with the predictions within bounds of a nominal and worst atmosphere as predicted by the OPALS link tool. Here the agreement to first order is very good though extending the analysis to more passes is pending. The particular pass chosen here covered a wide air-mass range and shows evidence of the piecewise agreement as pointed out earlier for mean beacon flux and normalized variance of the uplink.

Figure 8 shows the normalized variance for the July 21, 2014 nighttime pass and a July 22, 2014 daytime pass. The normalized variance is benign throughout the pass (see Figure 8). This is consistent with aperture averaging. It is not clear whether the slight increase in normalized variance observed is an atmospheric effect, firstly, because the daytime turbulence would be expected to be worse; and secondly, because the normalized variance of the APD noise in the absence of any signal (shown by circles) is strong. So the apparent increase in normalized variance may be an artifact of improving signal-to-noise ratio on the avalanche photo-diode (APD).

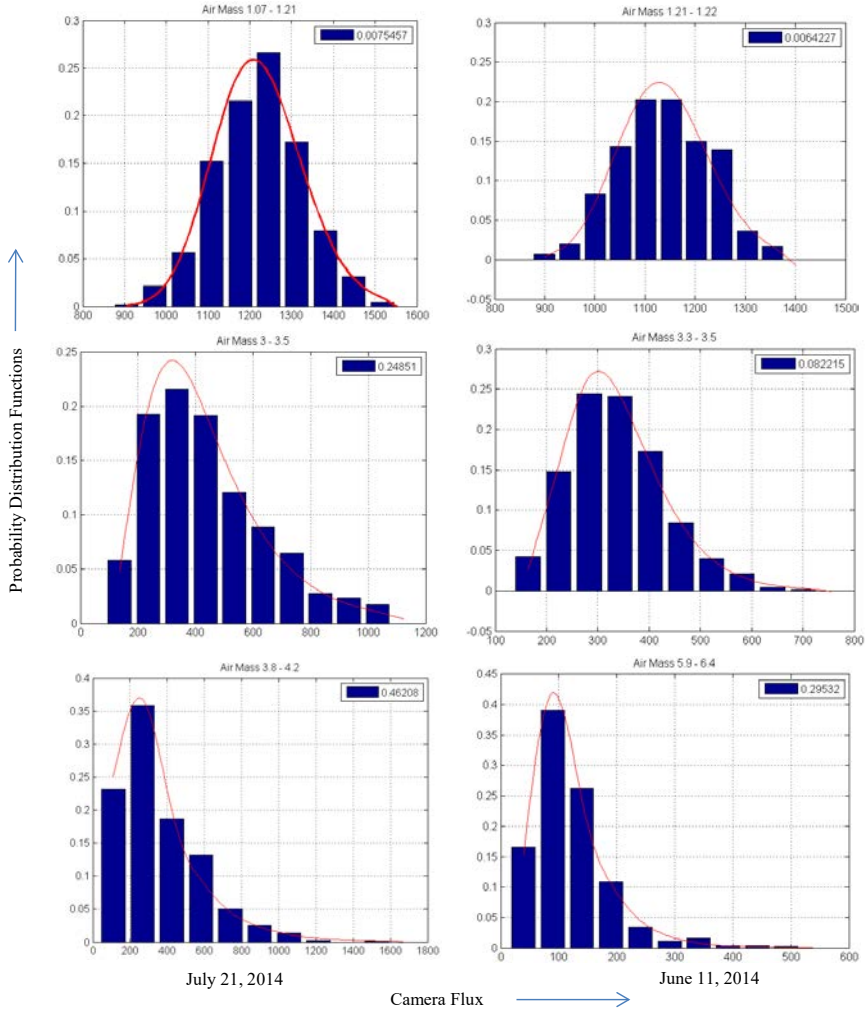


Figure 6. Comparison of the distribution of the OPALS camera flux of beacon

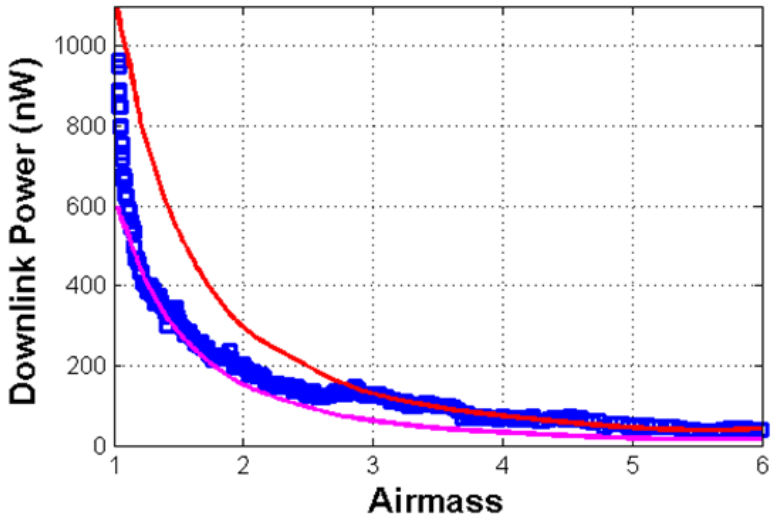


Figure 7. Downlink signal variation with air mass on July 21, 2014 compared to predicted bounds for different atmospheric attenuation expected at Table Mountain, CA.

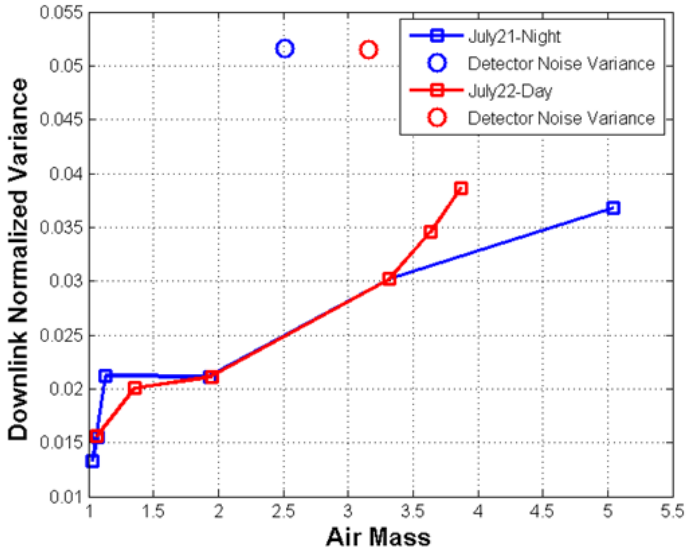


Figure 8. Normalized variance of the downlink measured by the avalanche photo-diode detector at the OPALS GS

The pass on June 6, with downlink performance data is shown in Figure 9. The data rate was 50 Mbps, and 120 seconds of data were recorded. The left plot contains one point per codeword as identified by the decoder's frame synchronizer. The left figure shows the number of the first symbol, and the number of bit errors, for each Reed-Solomon codeword. Many codewords were undecodable during the first 4.8 seconds as shown by crosses near the left hand upper border. A narrow gap is visible around symbol $0.3 \times 10^8$ where the frame synchronizer failed to find synchronization markers. For the remaining 15 seconds, the errors were rare and were all corrected. The right plot uses a moving average with a span of 0.4 seconds to extract the bit error rate. While bit errors were rare the curve shows stair-steps and statistics that are questionable, the error rate appears to be as low as $10^{-8}$ during the best part of the pass.

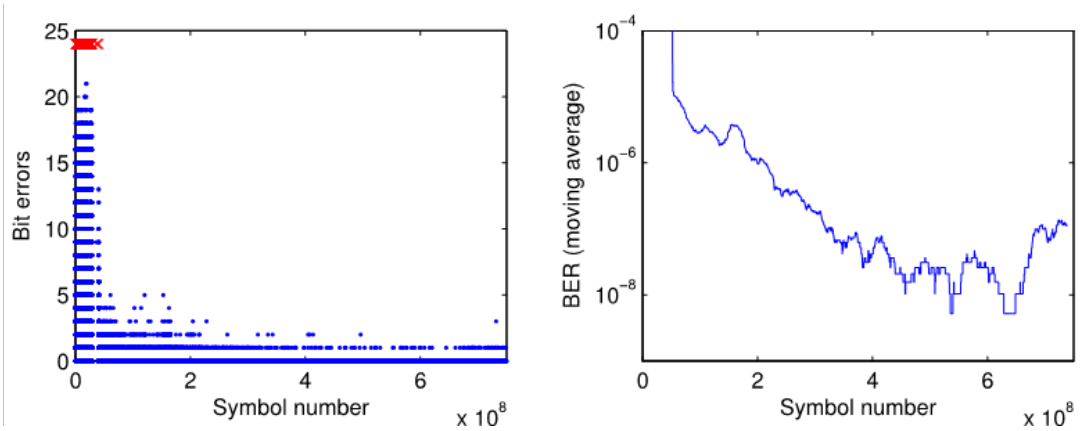


Figure 9. Downlink performance shown by the number of bit errors as a function of symbol number on the left and a running average of bite-error rate on the right. This was for a120 second pass on June 5, 2014.

## 4. CONCLUSIONS

Some link data gathered during the recently concluded OPALS demonstration of optical communication from the ISS to ground were presented. The link data was analyzed with the intent of reconciling the measurements with link predictions. The measurements analyzed showed good qualitative agreement with link predictions. The comparison with models also show that further study is needed to achieve a better understanding of the measurements relative to theoretical predictions. There is a hint in the data suggesting that atmospheric conditions over the range of air-masses used for measurements may be changing that needs further study.

In general OPALS was a low complexity approach to a link demonstration from a low earth orbiting ISS. The design and implementation was capability and cost driven without an imposition of performance requirements. The key requirement was to downlink a video from the ISS to the ground and the design addressed this. OPALS also exceeded this requirement by providing the opportunity to close links during daytime under diverse conditions in spite of a non-ideal spectral filter with 8 nm band-pass and a 8-bit camera with limited dynamic range and sampling rate. However, this strongly suggests the ability and readiness of free-space optical communications for downlinking huge data volumes for LEO spacecraft where many of the field-of-regard restrictions on the ISS would be removed allowing longer contact times. Narrowing of spectral band-pass and laser beam divergence will also support much higher data-rates.

The OPALS FS remains healthy at the time of writing this report and extended tests are planned.

## ACKNOWLEDGEMENTS

The authors would like to thank all members of the OPALS team present and past for their dedication and efforts which made the measurements reported here possible. The work described was carried out at the Jet Propulsion Laboratory (JPL), California Institute of Technology under contract with the National Aeronautics and Space Administration (NASA).

## REFERENCES

[1] Abrahamson, M., Sindiy, O., Oaida, B., Fregoso, S., Bowles-Martinez, J., Kokorowski, M., Wilkerson, W., and Konyha, A., "OPALS: Mission System Operations Architecture for an Optical Communications Demonstration on the ISS," SpaceOps 2014 13th International Conference on Space Operations, Pasadena, CA, 5-9 May 2014. AIAA-2014-1627.

[2] Oaida, B.V.; Kokorowski, M.; Erkmen, B.I.; Andrews, K.S.; Wu, W.; Wilkerson, M., “Impact of pointing performance on the optical downlink for the Optical PAyload for Lasercomm Science (OPALS) system” Proc. ICSOS 2014, S3-1, Kobe, Japan, May 7-9 (2014).

[3] Oaida, B.V.; Wu, W.; Erkmen, B.I.; Biswas, A.; Andrews, K.S.; Kokorowski, M.; Wilkerson, M., "Optical link design and validation testing of the Optical Payload for Lasercomm Science (OPALS) system," *Proc. SPIE 8971*, Free-Space Laser Communication and Atmospheric Propagation XXVI, 897131 (February 2014).
[4] Oaida, B.V.; Abrahamson, M.J.; Witoff, R.J.; Martinez, J.N.B.; Zayas, D.A., "OPALS: An optical communications technology demonstration from the International Space Station," *Aerospace Conference, 2013 IEEE* , vol., no., pp.1,20, 2-9 March 2013.
[5] Abrahamson, M. J., Bogdan O. V., Sindiy, O., Biswas, A., "Achieving operational two-way laser acquisition for OPALS payload on the International Space Station," Proc. SPIE 9354 (In Press).
[6] Abhijit Biswas, Joseph M. Kovalik, Bogdan Oaida, Matt Abrahamson and Malcolm W. Wright, "Upwelling Radiance at 976 nm Measured from Space Using a CCD Camera," Proc. SPIE 9354 (In Press).
[7] Kasten, F., and A. T. Young, "Revised optical air mass tables and approximation formula," Applied Optics 28, 4735–4738, 1989.
[8] Berk, A., Bernstein, L. S., Anderson, G. P., Acharya, P. K., Robertson, D. C., Chetwynd, J. H., Adler-Golden, S. M., "MODTRAN Cloud and Multiple Scattering Upgrades and Application to AVIRIS," Remote Sensing of Environment, 65(3), 367-375 (1998).